

The APPswe/PS1A246E mutations in an astrocytic cell line leads to increased vulnerability to oxygen and glucose deprivation, Ca²⁺ dysregulation and mitochondrial abnormalities

María Dolores Martin-de-Saavedra^{1,2,3*}, Elisa Navarro^{1,2}, Ana J. Moreno-Ortega^{1,2,4}, Mauricio P. Cunha⁵, Izaskun Buendia^{1,2}, Pablo Hernansanz-Agustín^{6,7}, Rafael León^{1,2,4}, María F. Cano-Abad^{1,2,4}, Antonio Martínez-Ruiz^{6,8}, Ricardo Martínez-Murillo⁹, Michael R. Duchon¹⁰ and Manuela G. López^{1,2}

¹Instituto Teófilo Hernando, Universidad Autónoma de Madrid, Madrid, España.

²Departamento de Farmacología y Terapéutica, Facultad de Medicina, Instituto de Investigación Sanitaria Princesa (IIS-IP), Universidad Autónoma de Madrid, Madrid, España. ³Department of Physiology, Northwestern University Feinberg School of Medicine, Chicago, Illinois, USA. ⁴Servicio de Farmacología Clínica, Instituto de Investigación Sanitaria Princesa (IIS-IP), Hospital Universitario de la Princesa, Madrid, España. ⁵Departamento de Bioquímica, Universidade Federal de Santa Catarina, Florianópolis, Brazil. ⁶Servicio de Inmunología, Instituto de Investigación Sanitaria Princesa (IIS-IP), Hospital Universitario de la Princesa, Madrid, España, ⁷Departamento de Bioquímica, Facultad de Medicina, Universidad Autónoma de Madrid (UAM) and Instituto de Investigaciones Biomédicas Alberto Sols, Madrid, España, ⁸Centro de Investigación Biomédica en Red de Enfermedades Cardiovasculares (CIBERCV), España, ⁹Instituto Cajal – CSIC. Madrid, España. ¹⁰Department of Cell and Developmental Biology, University College London, United Kingdom.

*To whom correspondence should be sent:

M. Dolores Martin-de-Saavedra, PhD

Northwestern University

303 E Chicago Ave

60611 Chicago, IL. USA

+13125031174

lola.mds@northwestern.edu

Running title: APP/PS1 mutations increase vulnerability to OGD/reox in astroglomas

Keywords: astrocytes, Alzheimer's disease, ischemia, mitochondrial dysfunction, calcium dyshomeostasis, cell death

Abbreviations:

AD, Alzheimer's Disease; APP, amyloid precursor protein; PS1, presenilin 1; OGD, oxygen and glucose deprivation; $[Ca^{2+}]$, calcium concentration; $[Ca^{2+}]_c$, cytosolic calcium concentration; $[Ca^{2+}]_{mit}$, mitochondrial calcium concentration; CNS, central nervous system; MTT, 3-(4,5-dimethylthiazol-2-yl)-2,5-diphenyltetrazolium bromide; LDH, lactate dehydrogenase; TMRE, Tetramethylrhodamine, ethyl ester, perchlorate; H₂DCFDA, 2', 7'- dichlorofluorescein diacetate; DCF, 2', 7'- dichlorofluorescein; WT, wild type; OGD/reox, Oxygen and glucose deprivation/reoxygenation; ROS, Reactive oxygen species; HBSS, Hanks's balanced salt solution; OCR, oxygen consumption rate; DMEM, Dulbecco's modified Eagle's Medium; F_t , fluorescence at a given time; F_0 , basal-fluorescence value before ATP injection; F_{max} , maximum fluorescence (Triton elicited); F_{min} , minimum fluorescence (MnCl₂ elicited); FCCP, carbonyl cyanide-4-(trifluoromethoxy)phenylhydrazone; InsP₃, inositol trisphosphate; AUC, area under the curve; SERCA, sarco/endoplasmic reticulum Ca²⁺-ATPase; ER, endoplasmic reticulum; CICR, Ca²⁺-induced Ca²⁺ release; CCE, capacitive Ca²⁺ entry; NCX, Na⁺/Ca²⁺ exchanger; PMCA, plasma membrane Ca²⁺ ATPase.

ABSTRACT

Growing evidence suggests a close relationship between Alzheimer's Disease (AD) and cerebral hypoxia. Astrocytes play a key role in brain homeostasis and disease states, while some of the earliest changes in AD occur in astrocytes. We have therefore asked whether mutations associated with AD increase astrocyte vulnerability to ischemia. Two astrogloma cell lines derived from APP_{SWE}/PS1A246E (APP, amyloid precursor protein; PS1, presenilin 1) transgenic mice and controls from normal mice were subjected to oxygen and glucose deprivation (OGD), an *in vitro* model of ischemia. Cell death was increased in the APP_{SWE}/PS1A246E line compared to the control. Increasing extracellular calcium concentration ($[Ca^{2+}]$) exacerbated cell death in the mutant but not in the control cells. In order to explore cellular Ca^{2+} homeostasis the cells were challenged with ATP or thapsigargin and $[Ca^{2+}]$ was measured by fluorescence microscopy. Changes in cytosolic Ca^{2+} concentration ($[Ca^{2+}]_c$) were potentiated in the APP_{SWE}/PS1A246E transgenic line. Mitochondrial function was also altered in the APP_{SWE}/PS1A246E astrogloma cells; mitochondrial membrane potential and production of reactive oxygen species were increased while mitochondrial basal respiratory rate and ATP production were decreased compared to control astrogloma cells. These results suggest that AD mutations in astrocytes make them more sensitive to ischemia; Ca^{2+} dysregulation and mitochondrial dysfunction may contribute to this increased vulnerability. Our results also highlight the role of astrocyte dyshomeostasis in the pathophysiology of neurodegenerative brain disorders.

INTRODUCTION

Many studies, including observational epidemiological studies, have proposed a relationship between vascular risk factors and Alzheimer's disease (AD). The link between AD and cerebrovascular disease has been documented by the following findings: (i) AD may increase the likelihood of suffering stroke and *vice versa* (Pluta 2004a, Pluta 2004b), (ii) the accumulation of the β amyloid peptide in the brain of AD patients leads to neuronal (Hardy & Selkoe 2002) and vascular toxicity (Paris *et al.* 2004a, Paris *et al.* 2004b) and also, (iii) AD and atherosclerosis share genetic and environmental risk factors such as ApoE ϵ 4 polymorphism, hypercholesterolemia, hypertension, obesity and metabolic syndrome, among others (Casserly & Topol 2004).

Astrocytes are the most abundant cells in the central nervous system (CNS). For decades, they were regarded as a passive supporting element in the brain, but this perception has dramatically changed in recent years. Astrocyte dysfunction seems to play a key role in the pathophysiology of many CNS diseases. For example, Verkhratsky *et al.* (Verkhratsky *et al.* 2010) have proposed the astrocyte as being potentially responsible for the early synaptic failure observed in AD. Besides the classical structural properties, astrocytes have metabolic, homeostatic, signaling and developmental functions. Astrocytes regulate the extracellular concentration of K^+ , glutamate, water and pH (Chen & Swanson 2003). They also encompass cerebral microcirculation with brain activity, as activity-induced Ca^{2+} transients in astrocytes are related to changes in vascular pressure and, thus, participate in regulating cerebral blood flow.

It has been reported that both human and mouse models of AD show astrogliosis at late stages of the disease (Olabarria *et al.* 2010, Nagele *et al.* 2003). However, at

early stages of the disease a degeneration/atrophy of these cells has been found in a triple transgenic mouse model of AD (Olabarria et al. 2010, Rodriguez *et al.* 2009). Moreover, during ischemia astrocytes take up excessive K⁺ and glutamate (Rothstein *et al.* 1996) and release trophic factors which limit the extent of stroke (Anderson *et al.* 2003, Swanson *et al.* 2004). After a stroke, astrocytes also play a crucial role in neuronal survival and recovery (Li *et al.* 2014). Nevertheless, if astrocytes are compromised, they might contribute to increase neuronal cell death and brain damage (Zhao & Rempe 2010).

Therefore, our aim was to study the role of astroglia in the relationship between AD and brain ischemia. We employed a control astroglioma cell line and another line harboring the APP^{swe}/PS1A246E AD-related mutations. We found that the AD mutated astroglial cell line showed increased vulnerability to oxygen and glucose deprivation; we also found altered Ca²⁺ homeostasis and impaired mitochondrial function in these cells, which may contribute to their vulnerability to ischemia.

MATERIALS AND METHODS

Materials

RPMI media and heat-inactivated bovine fetal serum were purchased from Invitrogen (Madrid, Spain). Penicillin/streptomycin and 3-(4,5-dimethylthiazol-2-yl)-2,5-diphenyltetrazolium bromide (MTT) were obtained from Sigma-Aldrich (Madrid, Spain). Lactate dehydrogenase (LDH) cytotoxicity detection kit was acquired from Roche Diagnostics (Mannheim, Germany). Tetramethylrhodamine, ethyl ester, perchlorate (TMRE), 2', 7'- dichlorofluorescein diacetate (H₂DCFDA), dihydroethidium, Fluo-4, Rhod-2 and Hoechst were purchased from Molecular Probes (Invitrogen, Madrid, Spain).

Culture and maintenance of astroglioma cell lines

The control and APP^{swe}/PS1A246E astroglioma cell lines were generated by injecting C57BL/6J wild type (WT) and APP^{swe}/PS1A246E mice with the carcinogen 20-methylcholanthrene (20-MT) in cortices as previously described (Serrano *et al.* 2010, Seyfried *et al.* 1992). Briefly, 9 month-old mice kindly donated Professor Ignacio Torres (Instituto Cajal, Madrid, Spain), were deeply anesthetized with pentobarbital (10 mg/kg) and atropine (90 mg/kg). Pellets of 20-MT were deeply implanted in the right parietal subcortex with the help of astereotaxic frame. Mice were observed periodically after the surgery and were sacrificed when their comfort or quality of life was compromised. The control cells correspond to the CT-2A cell line, which was kindly donated by Prof. Seyfried (Boston, MA, USA). For generating the APP^{swe}/PS1A246E cells, animals developed astrogliomas after 20-MT treatment, they were extracted, maintained in culture as a regular cell line and characterized (Ortega-Martinez 2015).

Both astrogloma cell lines were maintained in RPMI media supplemented with 10% of heat-inactivated fetal bovine serum (Invitrogen, Madrid, Spain), 4 U/mL penicillin and 4 µg/mL streptomycin (Sigma-Aldrich, Madrid, Spain). Cells were grown in flasks containing supplemented media, maintained at 37°C and 5% CO₂ humidified air and passed once *per* week. Control and APP^{swe}/PS1A246E cells were cultured in 48 well-plates at a seeding density of 20,000 cells *per* well. Cells were used after 48 hours at passages between 4 and 13 after thawing. Cell lines were last authenticated by immunofluorescence during the review process. Both cell lines showed specific astrocytic markers (vimentin, S100B and SOX2) and no neuronal markers (NeuN and MAP2) (Suppl. Fig. 2 and 3).

Oxygen and glucose deprivation/reoxygenation model

Oxygen and glucose deprivation/reoxygenation (OGD/reox) was used as an *in vitro* model of ischemia. For the OGD, the culture media was replaced by a solution containing (in mM): NaCl 137.93, KCl 5.36, CaCl₂ 2, MgSO₄ 1.19, NaHCO₃ 26, KH₂PO₄ 1.18 and 2-deoxyglucose 11 (Sigma-Aldrich) previously bubbled with a gas mixture containing 95% N₂/5% CO₂. Thereafter, cell plates were placed in an airtight chamber (Billups and Rothenberg, Inc) and were exposed for 5 min to 95% N₂/5% CO₂ gas flow to ensure purging of residual oxygen and the chamber was closed tightly and maintained at 37°C for 4 hours. Control cells were treated with a solution similar to the OGD solution but containing 15 mM glucose instead of 2-deoxyglucose and placed in a normoxic atmosphere during 4 hours. At the end of the 4 h OGD period, cells were withdrawn from the ischemia chamber and the OGD solution was replaced by control culture media and kept for a further 14 h in an incubator at 37°C in a humidified atmosphere (see protocol in **Fig. 1A**). At the end of the experiment, viability quantification by MTT and/or LDH was carried out. Reactive oxygen species (ROS)

levels were analysed by DCF fluorescence and mitochondrial membrane potential by TMRE staining.

Measurement of cell viability

Cell viability was measured using MTT (Sigma-Aldrich, Madrid, Spain) and lactate dehydrogenase (LDH) techniques. The MTT method is based in the ability of mitochondrial dehydrogenases of living cells to reduce MTT to produce a precipitated formazan, as previously described (Liu *et al.* 1997). MTT (5 µg/mL) was incubated during 2 hours at 37°C; then, the media was removed and the precipitated formazan was solubilized with 300 µl of dimethyl sulfoxide. Cellular viability was quantified spectrophotometrically at a wavelength of 550 nm. Basal condition, i.e. cells not exposed to OGD/reox, was considered as 100% viability and the rest of the variables were normalised with respect to that value.

Measurement of LDH activity was assessed using a cytotoxicity cell death kit (Roche Diagnostics, Mannheim, Germany) according to the manufacturer's instructions. LDH is a cytosolic enzyme that is released to the extracellular media in necrotic cell death. Extracellular and intracellular LDH were measured taking extracellular media or cellular lysates, respectively and total LDH activity was determined as the sum of extracellular plus intracellular measurements. Results were expressed as the percentage of extracellular LDH compared with total LDH activity.

Fluorescence assays

Mitochondrial membrane potential was assessed by TMRE (100 nM) fluorescence. TMRE is a positively-charged dye that accumulates within the relatively negative milieu of mitochondria leading to fluorescence emission at 574 nm when

excited at 549 nm. The more negative the mitochondrial membrane is, the more TMRE accumulates in the mitochondria, leading to an increase in fluorescence.

The fluorescent indicator H₂DCFDA was used to measure ROS production. Cells were incubated with 10 μM H₂DCFDA which is a cell-permeable dye that diffuses into cells. After entering into the cell, it is deacetylated by intracellular esterases and in the presence of ROS it is oxidized to dichlorofluorescein (DCF), a green fluorescent dye whose wavelengths of excitation and emission are 485 and 520 nm, respectively.

Results were normalised using the cell-permeable DNA stain Hoechst (1 μg/mL). Wavelengths of excitation and emission of Hoechst were 350 and 460 nm, respectively. Cells were equilibrated with all fluorescent dyes for 20 minutes at 37°C.

Fluorescence intensity was measured using an inverted NIKON eclipse T2000-U microscope (Nikon Instruments, Europe, Badhoevedorp, Netherlands). Images were taken at magnifications of 20x. Analysis of fluorescence imaging data was performed using Metamorph program version 7.0 (Molecular Devices, LLC, Sunnyvale, CA, USA). The average intensity of control cells in basal condition was considered 100% so that the rest of variables were normalised to this value.

Cytosolic Ca²⁺ measurements by fluorescence microscopy

The fluorescent Ca²⁺ indicator Fluo-4 AM was used to measure cytosolic-free Ca²⁺ levels in live cells. One day after seeding on Ø 22 mm cover slips and 50% confluency, cells were loaded with 5 μM Fluo-4 AM in the presence of 0.005% (w/v) pluronic acid (15 min incubation at RT~21 °C). The loading solution was then removed and cells were washed twice with modified Hanks' Buffered Salt Solution (HBSS 138 mM NaCl, 5.4 mM KCl, 0.25 mM Na₂HPO₄, 0.44 mM KH₂PO₄, 0.414 mM CaCl₂, 1.0 mM MgSO₄, 4.2 mM NaHCO₃, pH 7.4). Each cover slip was assembled into a purpose-

built chamber and a fresh aliquot of modified HBSS was added to the cells and placed on the stage of Zeiss 510 confocal laser scanning microscope. The temperature in the chamber of the microscope was maintained at 37°C. Images were acquired for 120 or 700 s using a HCX PLAPO 40X/1.25-0.75 oil immersion CS objective. Acquired images were analyzed with ImageJ (National Institutes of Health, USA). For thapsigargin/capacitative Ca²⁺ entry experiments, the cells were incubated first in modified HBSS without Ca²⁺. Following a recording time of 10 seconds, 1 μM thapsigargin was added to release Ca²⁺ from the endoplasmic reticulum (ER). Finally, 400 s thereafter 1 mM Ca²⁺ was introduced in the recording media eliciting a Ca²⁺ capacitative entry (CCE) response.

Measurement of mitochondrial oxygen consumption

Mitochondrial oxygen consumption rate (OCR) was assessed using the XF24 Extracellular Analyzer (Seahorse Bioscience, North Billerica, MA). Briefly, cells were plated in XF24 cell cultures microplates (Seahorse Bioscience) and cultured during 24 h in order to obtain a homogenous monolayer. For equilibration, cells were incubated with unbuffered Dulbecco's modified Eagle's Medium (DMEM) supplemented with 25 mM glucose, 1 mM pyruvate and 2 mM glutamine at 37°C in a CO₂-free incubator during 1 h prior to the experiment. A calibration cartridge (Seahorse Bioscience) was equilibrated overnight and afterwards loaded with unbuffered DMEM (port A) and 5 μg/ml oligomycin (port B) and 1 μM rotenone plus 1 μM antimycin A (port C), all obtained from Sigma-Aldrich (Madrid, Spain). Non-mitochondrial respiration was calculated as OCR after the administration of rotenone + antimycin and this value was subtracted to all measures. Basal respiration was calculated as the OCR after administration of unbuffered DMEM and ATP turnover as the difference between Basal Respiration and OCR after oligomycin administration. Results were normalized to total

protein content using Pierce BCA protein assay kit (Thermo Fisher Scientific, Madrid, Spain).

ATP measurement

ATP production was determined with an ATP Assay Kit (Fluorometric, ab83355, Abcam, Cambridge, United Kingdom). ATP production rate was determined following the protocol described by the manufacturer. Firstly, cells were washed with cold PBS and resuspended in 100 μ l of ATP assay buffer. Then, the cells were quickly homogenized by pipetting up and down, centrifuged for 2 min at 4°C (13,000 rpm) to remove any insoluble material. Thereafter, the supernatant was collected and transferred to a clean tube and kept on ice. 400 μ l of ATP assay buffer and 100 μ l of ice-cold perchloric acid (4 M) were added to the homogenate to deproteinate the samples. The homogenates were vortexed briefly and incubated on ice for 5 minutes. The homogenate was centrifuged at 13,000 rpm for 2 min at 4°C and the supernatant was transferred to a fresh tube. The supernatant volume was measured and an equal volume of ice-cold 2 M KOH was added. Finally, the homogenate was centrifuged at 13,000 rpm 15 min at 4°C and the supernatant was collected. 50 μ l of ATP reaction mix and 50 μ l of sample were added to each well and incubated at room temperature for 30 min, protected from light. The samples were measured on a microplate reader at 535/587 nm.

Mitochondrial and cytosolic Ca²⁺ assays using a microplate reader

Cells were plated in bottom transparent 96-well black plates and cultured during 24 h at 37°C. Before the experiment, cells were loaded with 5 μ M Fluo-4 AM (to measure cytosolic Ca²⁺ levels) or 3 μ M Rhod-2 AM (to measure mitochondrial Ca²⁺ levels) (Thermo Fisher Scientific, Madrid, Spain) in non-supplemented RPMI media (+ 0.005% w/v pluronic acid) for 1 h at 37°C. Afterwards, cells were washed twice with

Krebs-HEPES solution (in mM): 140 NaCl, 5.6 KCl, 1.2 MgCl₂, 0.4 CaCl₂, 10 HEPES, 11 D-glucose, pH 7.4. To induce cytosolic and mitochondrial Ca²⁺ increases, a concentrated solution of ATP was injected to each well to obtain a final concentration of 10 μM. Fluorescence measurements were carried out using a microplate reader (FLUOstar Optima, BMG, Germany). Wavelengths of excitation and emission were 494/506 nm (Fluo-4 AM) and 552/581 nm (Rhod-2 AM), respectively. At the end of the experiment, 5 % triton and 1mM MnCl₂ were added to each well to calculate maximum fluorescence (F_{max}) and minimum fluorescence (F_{min}) respectively. ATP-induced responses were expressed as a percentage of the fluorescence value at each time point (% F_t). This was calculated by subtracting the fluorescence at a given time (F_t) to the basal-fluorescence value before ATP injection (F₀) and divided by the F_{max}-F_{min} fluorescence, calculated using the following formula:

$$\% F_t = (F_t - F_0) / (F_{\max} - F_{\min}) * 100$$

The maximum % fluorescence intensity for Fluo-4 (Maximum % [Ca²⁺]_c) and Rhod-2 (Maximum [Ca²⁺]_{mit}) were obtained for each experiment. All experiments were performed in triplicates and replicated 4 times.

Statistical analysis

Statistical analysis was performed using GraphPad Prism 5.0 (La Jolla, USA). To compare differences between two groups, Student's *t*-test (Gaussian distribution of data) or Mann Whitney test (non-Gaussian distribution of data) were used. Data distribution was considered Gaussian after passing the Kolmogorov-Smirnov test or the *F*-test to compare variances when *n*<5. To compare multiple variables, two-way ANOVA was used, followed by a Bonferroni *post hoc* test to compare replicate means. Statistical differences were considered when *P*<0.05.

RESULTS

1. Vulnerability of APP^{swe}/PS1A246E astroglia cells to OGD/reoxygenation

To study the influence of AD mutations on astroglial responses to an ischemic episode, we exposed control and APP^{swe}/PS1A246E mutated astroglial cell lines to oxygen and glucose deprivation followed by reoxygenation (OGD/reox). Both cell lines were subjected to 4 h of OGD followed by 14 hours of reoxygenation (**Fig. 1A**). Cell viability was measured as LDH released into the extracellular media and MTT metabolism. The OGD/reox paradigm increased cell death far more in the APP^{swe}/PS1A246E cells than in controls; LDH release was increased by 25% and MTT reduction was decreased by 40%, while in the control cell line LDH release was increased by 11% and MTT metabolism was unchanged (**Fig. 1C and D**). Thus, APP^{swe}/PS1A246E mutations increased astrocyte vulnerability to ischemia. In line with these results, bright field microphotographs (**Fig. 1B**), showed a decrease in cell number in APP^{swe}/PS1A246E cells when compared to control after OGD/reox. In the analysis of % LDH release after OGD/reox (**Fig. 1C**), the two-way ANOVA revealed a significant effect of treatment [$F_{1,12} = 42.11$, $P < 0.01$], a significant effect of genotype [$F_{1,12} = 5.382$, $P < 0.05$] and a significant treatment \times genotype interaction [$F_{1,12} = 1.334$, $P > 0.05$]. In the analysis of % MTT metabolism after OGD/reox (**Fig. 1D**), the two-way ANOVA revealed a significant effect of treatment [$F_{1,14} = 16.57$, $P < 0.01$], a significant effect of genotype [$F_{1,14} = 7.214$, $P < 0.05$] and a significant treatment \times genotype interaction [$F_{1,14} = 7.214$, $P > 0.05$]. It should be noted that similar results were obtained with LDH and MTT assays. Given the simplicity of the method we decided to use this technique in the following experiments.

To study this phenomenon further, both astrogloma cell lines were subjected to the OGD/reox protocol and afterwards mitochondrial membrane potential and rates of ROS generation were measured by fluorescence microscopy. In basal conditions the TMRE fluorescence was 2-fold greater in APP^{swe}/PS1A246E than in control cells (**Fig. 1E**), indicating an increased mitochondrial membrane potential; while the rate of ROS generation was increased by almost 3-fold (**Fig. 1F**). After OGD/reox, control or APP^{swe}/PS1A246E did not show a significant increase in TMRE fluorescence when compared to their respective basal conditions (**Fig. 1E**). However, the production of free radicals after OGD/reox was potentiated in the APP^{swe}/PS1A246E astrogloma cell line by 3-fold when compared to control cells after OGD/reox, demonstrating significant positive interaction between the presence of the mutation and ROS production (**Fig. 1F**). Of note, we assessed whether TMRE was working in non-quenching mode by adding carbonyl cyanide-4-(trifluoromethoxy)phenylhydrazone (FCCP) and oligomycin to the cultures (data not shown). In the analysis of TMRE fluorescence after OGD/reox (**Fig. 1E**), the two-way ANOVA revealed a significant effect of treatment [$F_{1,24} = 5.242$, $P < 0.05$], a significant effect of genotype [$F_{1,24} = 15.96$, $P < 0.001$] and no treatment \times genotype interaction [$F_{1,24} = 0.332$, $P > 0.05$]. In the analysis % DCF/Hoechst fluorescence after OGD/reox (**Fig. 1F**), the two-way ANOVA revealed a significant effect of treatment [$F_{1,27} = 30.46$, $P < 0.001$], a significant effect of genotype [$F_{1,27} = 28.24$, $P < 0.001$] and a significant treatment \times genotype interaction [$F_{1,27} = 5.546$, $P < 0.05$].

2. Ca²⁺-dependent cell death in the APP^{swe}/PS1A246E astrogloma cell line

Ca²⁺ plays a major role both in the pathophysiology of and cell death associated with AD and stroke. It is also a second messenger that allows astroglial cells to communicate through the astrocytic network by propagating Ca²⁺ waves (**Sheppard *et***

al. 1997). We therefore explored the role of Ca^{2+} in the vulnerability to ischemia of the cells expressing APP_{swe}/PS1A246E mutations. We performed the OGD/reox experiments increasing the concentration of extracellular Ca^{2+} from 0.414 mM (the Ca^{2+} concentration in RMPI media) to 5 mM (**Fig. 2A**). As previously observed (**Fig. 1D**), the vulnerability of APP_{swe}/PS1A246E cells to OGD/reox was greater than that of control cells. Furthermore, this vulnerability was dependent on the extracellular concentration of Ca^{2+} (**Fig. 2B**): increasing extracellular Ca^{2+} concentration was to 5 mM, significantly decreased cell viability by 18% in the APP_{swe}/PS1A246E cells compared to the 0.414 mM Ca^{2+} + OGD/reox group, while it had no significant impact on viability of control cells. Moreover, the difference in cell viability at 0.4 mM Ca^{2+} + OGD/reox between control and APP_{swe}/PS1A246E cells was 17%, whereas it increased to 27% at 5 mM Ca^{2+} +OGD/reox. In **Fig. 2B**, the two-way ANOVA revealed a significant effect of calcium [$F_{2,12} = 31.38$, $P < 0.001$], a significant effect of genotype [$F_{2,12} = 9.563$, $P < 0.05$] and a significant calcium \times genotype interaction [$F_{2,12} = 5.796$, $P > 0.05$]. Therefore, these results show that the increased vulnerability to OGD/reox in the APP_{swe}/PS1A246E cell line reflects impaired regulation of Ca^{2+} homeostasis, demonstrated by a statistical difference in the interaction between calcium \times genotype in the two-way anova, although other mechanisms cannot be ruled out.

3. APP_{swe}/PS1A246E mutation alters intracellular Ca^{2+} signaling

To determine whether Ca^{2+} homeostasis was altered in the APP_{SWE}/PS1A246E astrogloma cell line, cells were stimulated with different concentrations of ATP (1, 10, 100 μM) and cytosolic Ca^{2+} levels were measured. ATP releases Ca^{2+} from the ER through activation of inositol trisphosphate (InsP₃) receptors, which is the main Ca^{2+} signaling pathway in astrocytes. Cytosolic Ca^{2+} was measured in Fluo-4 AM loaded cells. 1 μM ATP generated a cytosolic Ca^{2+} transient in APP_{swe}/PS1A246E cells but

not in control cells, indicating that APP_{SWE}/PS1A246E mutated astrogloma cells are more sensitive to InsP₃ receptor signaling (**Fig. 3A**). ATP at 10 μ M and 100 μ M increased cytosolic Ca²⁺ in both cell lines (**Fig. 3B** and **3C**); nevertheless, the maximal [Ca²⁺]_c peak values (**Fig. 3D**), the area under the curve (AUC) (**Fig. 3E**) and the width (**Fig. 3F**) of the intracellular Ca²⁺ transients were all increased in the APP_{swe}/PS1A246E cells. Furthermore at the end of the measurement period (120 seconds), the basal cytoplasmic Ca²⁺ levels had still not returned to baseline in the APP_{swe}/PS1A246E cells. In the maximal peak analysis (**Fig. 3D**), the two-way ANOVA revealed a significant effect of ATP [$F_{1,21} = 31.38$, $P < 0.001$], a significant effect of genotype [$F_{3,21} = 27.81$, $P < 0.001$] and a significant ATP \times genotype interaction [$F_{3,21} = 4.294$, $P < 0.05$]. In the AUC analysis (**Fig. 3E**), the two-way ANOVA revealed a non-significant effect of ATP [$F_{1,9} = 0.067$, $P > 0.05$], a significant effect of genotype [$F_{1,9} = 44.09$, $P < 0.0001$] and no ATP \times genotype interaction [$F_{1,9} = 0.198$, $P > 0.05$]. In the width analysis (**Fig. 3F**), the two-way ANOVA revealed a non-significant effect of ATP [$F_{1,9} = 0.1441$, $P > 0.05$], a significant effect of genotype [$F_{1,9} = 22.38$, $P < 0.01$] and no ATP \times genotype interaction [$F_{1,9} = 8.570e-005$, $P > 0.05$].

To further study the differences observed in Ca²⁺ homeostasis, control and APP_{swe}/PS1A246E cell lines were exposed to thapsigargin to measure endoplasmic reticulum (ER) stored Ca²⁺. By blocking the sarco/endoplasmic reticulum Ca²⁺-ATPase (SERCA) pump, thapsigargin produces a [Ca²⁺]_c signal derived from Ca²⁺ release through ER leak channels, which may be amplified by Ca²⁺-induced Ca²⁺ release (CICR). The kinetics of the response were strikingly faster in APP_{swe}/PS1A246E astrogloma cells (**Fig. 4A**), although there was no significant difference in the AUC ($t_{11}=1.8$, $P=0.073$, **Fig. 4B**): there was a 40% decrease in T_{max} ($U=0.0$, $P=0.0012$, **Fig.**

4C), more than a 2-fold decrease in peak width ($t_{11}=8.8$, $P<0.0001$, **Fig. 4D**) and a 2.5-fold increase in the maximal peak ($t_{11}=11.74$, $P<0.0001$, **Fig. 4E**). On the other hand, capacitive Ca^{2+} entry (CCE) was not significantly different in the two astroglioma cell lines in terms of maximal peak ($t_8=1.869$, $P=0.0985$, **Fig. 4F**). However, cytoplasmic Ca^{2+} levels remained higher in astroglioma cells carrying the mutation (final steady state) at the end of the experiment ($U=3.00$, $P=0.0152$, **Fig. 4G**). In order to analyze whether this change in Ca^{2+} homeostasis is detrimental for the APP^{swe}/PS1A246E, we measured cell viability after incubating the cells with the same concentration of thapsigargin overnight. Interestingly enough, only the APP^{swe}/PS1A246E cells showed an increase in cell death (2-fold increase) after thapsigargin treatment (**Fig. 4H**). Taken together, these results would further suggest that the increased vulnerability to OGD/reox found in APP^{swe}/PS1A246E astroglioma cell line seems to be related to Ca^{2+} dysregulation. In the statistical analysis of % LDH release after thapsigargin treatment (**Fig. 3F**), the two-way ANOVA revealed a non-significant effect of treatment [$F_{1,20} = 8.17$, $P = 0.0097$], a significant effect of genotype [$F_{1,20} = 9.216$, $P = 0.0065$] and no treatment \times genotype interaction [$F_{1,20} = 3.579$, $P > 0.05$].

4. Mitochondrial function is impaired in APP^{swe}/PS1A246E mutated astroglioma cells

The main mechanisms regulating cytosolic Ca^{2+} levels are the intracellular stores (ER and the mitochondria), cytosolic Ca^{2+} binding proteins that buffer [Ca^{2+}] and Ca^{2+} extrusion mechanisms such as the plasma membrane Ca^{2+} ATPase (PMCA) proteins or the $\text{Na}^+/\text{Ca}^{2+}$ exchanger (NCX). Furthermore, in AD or in response to beta amyloid, mitochondrial respiration is impaired, ROS generation is increased and mitochondrial membrane potential is altered (Abramov *et al.* 2004, Casley *et al.* 2002, Abeti *et al.* 2011). As we already found that basal ROS levels and TMRE fluorescence were

increased in the APP^{swe}/PS1A246E cell line, we measured different aspects of mitochondrial function.

Firstly, to assess whether mitochondrial Ca²⁺ handling was perturbed in the APP^{swe}/PS1A246E cells, we measured [Ca²⁺]_c and mitochondrial Ca²⁺ concentration ([Ca²⁺]_{mit}) levels on exposure to 10 μM ATP. Surprisingly, we did not observe differences in [Ca²⁺]_{mit} responses between the cell lines ($t_6=0.9060$, $P=0.3998$, **Fig. 5A and B**) measured by Rhod-2 fluorescence. However, [Ca²⁺]_c levels were increased in the APP^{swe}/PS1A246E mutated cells in accordance with our previous experiments ($U=0.0$, $P=0.0286$, **Fig. 5C and 5D**).

We also measured the rate of oxygen consumption in both cell lines and found that the mutations were associated with a decrease in basal respiration ($t_6=7.104$, $P=0.0004$, **Fig. 5E and H**) and coupled respiration ($t_6=5.474$, $P=0.0016$, ATP turnover, **Fig. 5F and H**). Furthermore, ATP production in APP^{swe}/PS1A246E cells was significantly reduced compared to control cells ($t_4=2.156$, $P=0.0973$, **Fig. 5G and H**).

Taken together, APP^{swe}/PS1A246E cells showed mitochondrial dysfunction that might contribute to an increased vulnerability to OGD/reox. Moreover, taking into account: (i) the mitochondrial membrane hyperpolarization, (ii) the increased ROS production and (iii) the decreased ATP levels found in APP^{swe}/PS1A246E cell line, we hypothesize that these results could be due to impaired activity of the ATP synthase.

DISCUSSION

We have found that an astrocytic cell line carrying the APP^{swe}/PS1A246E mutations is more vulnerable to ischemia. They also present altered calcium signals and mitochondrial dysfunction that might contribute to the increased sensibility to ischemia.

The relationship between AD and ischemia has been well documented previously (Gorelick 2004, Casserly & Topol 2004). Coexistence of stroke and AD occurs more than by chance alone and they are known to exacerbate each other (Kalaria *et al.* 1993, Pasquier *et al.* 1998). On the other hand, interest in the role of astrocytes in stroke and AD has been growing in recent years with increasing evidence that they contribute significantly to the progression of both diseases (Verkhatsky *et al.* 2010, Anderson *et al.* 2003, Swanson *et al.* 2004, Li *et al.* 2014). Thus, we aimed to find whether AD mutations could compromise astrocyte function in such a way that they are more vulnerable to ischemia and so clarify the potential role for astrocyte pathophysiology in the relationship between AD and stroke.

To address this question, we chose two astrogloma cell lines, control and APP^{swe}/PS1A246E, derived from WT and APP^{swe}/PS1A246E mice, respectively. Interestingly, the cell line expressing both mutations associated with familial AD, showed higher vulnerability to the ischemia-reperfusion stimulus compared to the control cell line (**Fig. 1C and D**). This higher vulnerability to ODG/reox was accompanied by higher mitochondrial membrane potential and increased ROS production (**Fig. 1E and F**). In line with our results, Zhen *et al.* also observed increased cell death in hippocampal slices subjected to OGD in APP^{swe}/PS1 Δ E9 mice compared to wild type mice and in the CA1 region of the same mice that underwent global cerebral ischemia (Zhen *et al.* 2012). Astrocytes are relatively resistant to hypoxia

(Panickar & Norenberg 2005), thus it is not surprising that the control cell line was not affected by the OGD/reox protocol defined by MTT metabolism. However, it is worth noting that astrocytic cell death has also been observed in wild type astrocytes in models of ischemia *in vivo* (Li *et al.* 1995, Chen *et al.* 1997) and that the contribution of this cell type to excitotoxicity after ischemia has been previously documented (Rossi *et al.* 2000). The increased vulnerability of APP^{swe}/PS1A246E astrocytes to the ischemic insult could be related to the higher incidence of stroke in AD patients and highlights the possible role of astrocytes in these pathological events. As Ca²⁺ plays a major role in cell death associated with AD and stroke (Lee *et al.* 1999, Weiss *et al.* 1994, Schneider *et al.* 2001, Begley *et al.* 1999, Goldberg & Choi 1993), we performed the same experiment but increasing the concentration of extracellular Ca²⁺ and observed a potentiation of cell death in the AD mutated cell line (**Fig. 2**), highlighting the role of Ca²⁺ signaling in OGD/reox vulnerability in the mutated cell line.

Given that APP and PS1 mutations have been described to affect Ca²⁺ homeostasis in different cell models (Guo *et al.* 1996, Guo *et al.* 1997, Johnston *et al.* 2006) we decided to study Ca²⁺ regulation in both cell lines. When ATP was used to trigger ER Ca²⁺ release mediated by InsP₃, the mutated cell line responded with an increased cytoplasmic [Ca²⁺] with increased maximal peak, AUC and width (**Fig. 3**). Our results agree with studies reported by Grolla *et al.* (Grolla *et al.* 2013) in which the authors reported that cytoplasmic Ca²⁺ levels after stimulation of neuron-glia co-cultures with a metabotropic receptor agonist were increased in cultures treated with beta amyloid. Interestingly enough, the lowest concentration used in this study (1 μM ATP), elicited a Ca²⁺ signal in APP^{swe}/PS1A246E but not in the control cell line which points to an increased response to this pathway. Supporting our data, Johnston *et al.*, described that astrocytes transfected with a PS1 harbouring a mutation linked to familial

AD, showed Ca^{2+} oscillations at lower ATP and glutamate concentrations compared to astrocytes transfected with wild type PS1 (Johnston et al. 2006). To corroborate the alteration in Ca^{2+} regulation after ATP incubation, we induced the release of Ca^{2+} from the ER by blocking the SERCA pump through thapsigargin treatment. Again, we observed an increase in the maximal peak but this time due to a change in kinetics rather than to an increased overall Ca^{2+} release, as there were no changes in the AUC, but the width and the T_{max} were decreased (**Fig. 4**). After depleting the intracellular stores of Ca^{2+} , we re-added Ca^{2+} to the extracellular solution to activate CCE. We observed an increase in the final height and, interestingly, the decay of the signal in the APP_{swe}/PS1A246E cell line seemed to be decreased, which may be due to a failure in Ca^{2+} extrusion to the extracellular media. Taken together, these data show that APP_{swe}/PS1A246E mutations lead to increased Ca^{2+} concentration in the cytosol after stimulation. These results are of particular interest as Ca^{2+} signaling in astrocytes has been postulated to contribute to the progression of AD (Gomez-Gonzalo *et al.* 2017). Excessive Ca^{2+} responses are known to lead to apoptotic and necrotic cell death, which is demonstrated by the fact that thapsigargin induced Ca^{2+} cell death in APP_{swe}/PS1A246E cell line but not in the control (**Fig. 4H**).

Mitochondrial abnormalities in the APP/PS1 mouse model have been widely studied by several authors in cultured neurons (Sompol *et al.* 2008), brain slices (Dragicevic *et al.* 2011), or isolated brain mitochondria (Dragicevic *et al.* 2011), although the role of astrocytes on this issue has been less explored. Thus, we decided to study mitochondrial function in our experimental setting. We found that the astrogloma cells carrying the APP_{swe}/PS1A246E mutations displayed mitochondrial membrane hyperpolarization and increased ROS levels (**Fig. 1E and F**). They also showed a decrease in ATP levels (**Fig. 5G**). The increased mitochondrial membrane potential in

APP^{swe}/PS1A246E cells may support increased ROS production, as described elsewhere (Lee *et al.* 2002). Interestingly, iPSC-derived neurons with the 10+ 16 *MAPT* mutation, which induces an increase in the production of 4R tau isoforms, leads to mitochondrial hyperpolarization, ROS overproduction, lower ATP production and altered bioenergetics (Esteras *et al.* 2017), similar to the results described in this study. Altogether, these data indicate that the APP^{swe}/PS1A246E mutations might inhibit ATPase synthase activity, which would increase mitochondrial membrane potential, increase ROS production and decrease ATP production. Several studies have found a decrease in the activity of the mitochondrial ATPase synthase in AD (Beck *et al.* 2016, Cha *et al.* 2015). Schmidt *et al.* have identified APP as a binding partner of the alpha subunit of the mitochondrial ATP synthase (Schmidt *et al.* 2008) and A β interacts with oligomycin sensitivity conferring protein (OSCP), component of the ATPase synthase, leading to a loss-of-function (Beck *et al.* 2016). Moreover, an abnormal accumulation of APP has been found in the mitochondria of AD patients (Devi *et al.* 2006). Thus, APP or A β could be abnormally regulating mitochondrial ATPase synthase activity in the APP^{swe}/PS1A246E cells by directly binding to it and decreasing its activity.

Finally, taking into account mitochondrial dysfunction associated with AD mutations and their implication in Ca²⁺ homeostasis, we aimed to compare Ca²⁺ responses in cytosol and mitochondria in both cell lines. Interestingly enough, the Ca²⁺ transients observed in the mitochondria after ATP stimulation did not differ between control and APP^{swe}/PS1A246E astrocytic cell lines. Thus, cell death may not be due to Ca²⁺ overload in the mitochondria but due to Ca²⁺ overload in the cytosol. Of note, it has been described that cytosolic Ca²⁺ overload leads to cell death by overactivating the proteolytic enzyme calpain leading to fragility and rupture of the plasma and ER membrane (Garcia-Dorado *et al.* 2012, Murphy *et al.* 2014). However, compromised

mitochondrial function through increased ROS production and a hyperpolarized membrane potential may also participate in this process.

In conclusion, we have found that astrocytes carrying the APP^{swe}/PS1A246E exert alterations in calcium regulation and mitochondrial function which could contribute to the increased vulnerability to OGD/reox. Thus, AD mutations may alter the normal physiology of astrocytes, to the extent that they are vulnerable to stimuli that are harmless in healthy conditions with the obvious impact for neuronal function and survival. However, these results still need further confirmation in primary cultures and in an *in vivo* model.

CONFLICT OF INTEREST

The authors have no conflicts of interest to declare in relation to this manuscript.

ACKNOWLEDGEMENTS

This work was supported by the Spanish Government (partially funded by the European Union ERDF/FEDER) Ref. SAF2015-63935R to M.G.L.; Ref. SAF2015-65586 to R.M.M; Ref. PI15/00107 to A.M.R.; FPU/contract Ref. AP2009/0343 to A.J.M.O., the Spanish Ministry of Health (Instituto de Salud Carlos III) Ref. PI14/00372 to R.L and a grant from the Fundación Domingo Martínez (Spain) to A.M.R. and M.G.L. R.L. thanks the Instituto de Salud Carlos III and the European Regional Development's funds (FEDER) for a research contract under the Miguel Servet II Program (CPII16/00014). We also thank the Fundación Teófilo Hernando for its continuous support.

FIGURE LEGENDS

Figure 1. Increased vulnerability of APP^{swe}/PS1A246E astrogloma cells to oxygen and glucose deprivation/reoxygenation. (A) Experimental procedure: after 48 hours in culture, cells were exposed for 4 h to normoxic saline solution with glucose (Basal), or to oxygen and glucose deprivation (OGD) solution; thereafter, the incubation media was changed for RPMI media for 14 h (reox). (B) Representative images of both control and APP^{swe}/PS1A246E cells, under basal or OGD/reox conditions. Quantification of cell viability by LDH (C) and MTT (D). Quantification of fluorescent intensity in cells stained with TMRE (E) and H₂DCFDA (F). Data are shown as means and S.E.M. of n=3-8 independent experiments. Two-way ANOVA + Bonferroni *post hoc*. **P*<0.05, ****P*<0.001 vs basal situation; #*P*<0.05, ##*P*<0.01, ###*P*<0.001 vs control cell line. Two-way ANOVA + Bonferroni *post hoc*. Each “n” represents an independent experiment, corresponding to different passages of the cell lines.

Figure 2. Cell vulnerability upon oxygen and glucose deprivation/reoxygenation is Ca²⁺-dependent in APP^{swe}/PS1A246E cells. (A) Experimental procedure: after 48 hours in culture, cells were exposed to normoxic saline solution with glucose (Basal) for 4 h, or to oxygen and glucose deprivation solution (OGD) in the presence of increasing concentrations of extracellular Ca²⁺ (0.4, 5 mM); thereafter, the incubation media was changed for RPMI media for 14 h containing also increasing concentrations of extracellular Ca²⁺ (0.4, 5 mM). (B) Quantification of cell death after OGD/reox ± 0.4 and 5 mM Ca²⁺ measured by MTT metabolism. Data are shown as means and S.E.M. of n=4 independent experiments. Two-way ANOVA + Bonferroni *post hoc*. **P*<0.05, ****P*<0.001 vs basal situation; #*P*<0.05. Two-way ANOVA + Bonferroni *post hoc*. Each “n” represents an independent experiment, corresponding to different passages of the cell lines.

Figure 3. Cytosolic Ca²⁺ levels elicited by ATP are increased in APP^{swe}/PS1A246E cells. Representative [Ca²⁺]_c transients evoked by ATP 1 μM (A), 10 μM (B) and 100 μM (C) recorded in control and APP^{swe}/PS1A246E astrogloma cells. Quantification of the maximal peak (D), area under the curve (E) and width (F) in both cell lines stimulated with different concentrations of ATP. Data are shown as means and S.E.M (n=3-4 independent experiments). **P*<0.05, ***P*<0.01, ****P*<0.001 vs control. Two-way ANOVA + Bonferroni *post hoc*. Each “n” represents an independent experiment, corresponding to different passages of the cell lines.

Figure 4. The APP^{swe}/PS1A246E astrogloma cell line shows higher vulnerability to thapsigargin. Representative curves of cytoplasmic Ca²⁺ levels measured by Fluo-4 (A). Quantification of kinetic parameters of endoplasmic reticulum Ca²⁺ release after activation with thapsigargin: area under the curve (B), T_{max} (C), Width (D) and peak (E). Quantification of capacitative Ca²⁺ entry (CCE) kinetic parameters peak (F) and final height (G). Data are shown as means and S.E.M. (4-7 experiments). **P*<0.05, ****P*<0.001 vs control. Student’s *t*-test. (H) APP^{swe}/PS1A246E show increased LDH release after incubating the cells with 1 μM thapsigargin overnight. Data are shown as means and S.E.M. (n=6 experiments). ***P*<0.01, vs control+thapsigargin group; ###*P*<0.01 vs APP^{swe}/PS1A246E basal. Two-way ANOVA + Bonferroni *post hoc*. Each “n” represents an independent experiment, corresponding to different passages of the cell lines.

Figure 5. APP/PS1 mutations lead to mitochondrial dysfunction in astrogloma cells. Representative curve of [Ca²⁺]_{mit} levels measured by Rhod-2 (A) and [Ca²⁺]_c levels measured by Fluo-4 (C) fluorescence after 10 μM ATP addition and its quantification (B and D). (E) Mitochondrial basal respiration, (F) ATP turnover and (G)

ATP levels in both control and APP^{swe}/PS1A246E astrogloma cell lines. Representative graph of oxygen-consumption rate for control cells and APP^{swe}/PS1A246E (H). Data are shown as means and S.E.M. of n=3-4 independent experiments. ** $P < 0.01$, *** $P < 0.001$ vs control. Student's *t*-test. Each "n" represents an independent experiment, corresponding to different passages of the cell lines.

REFERENCES

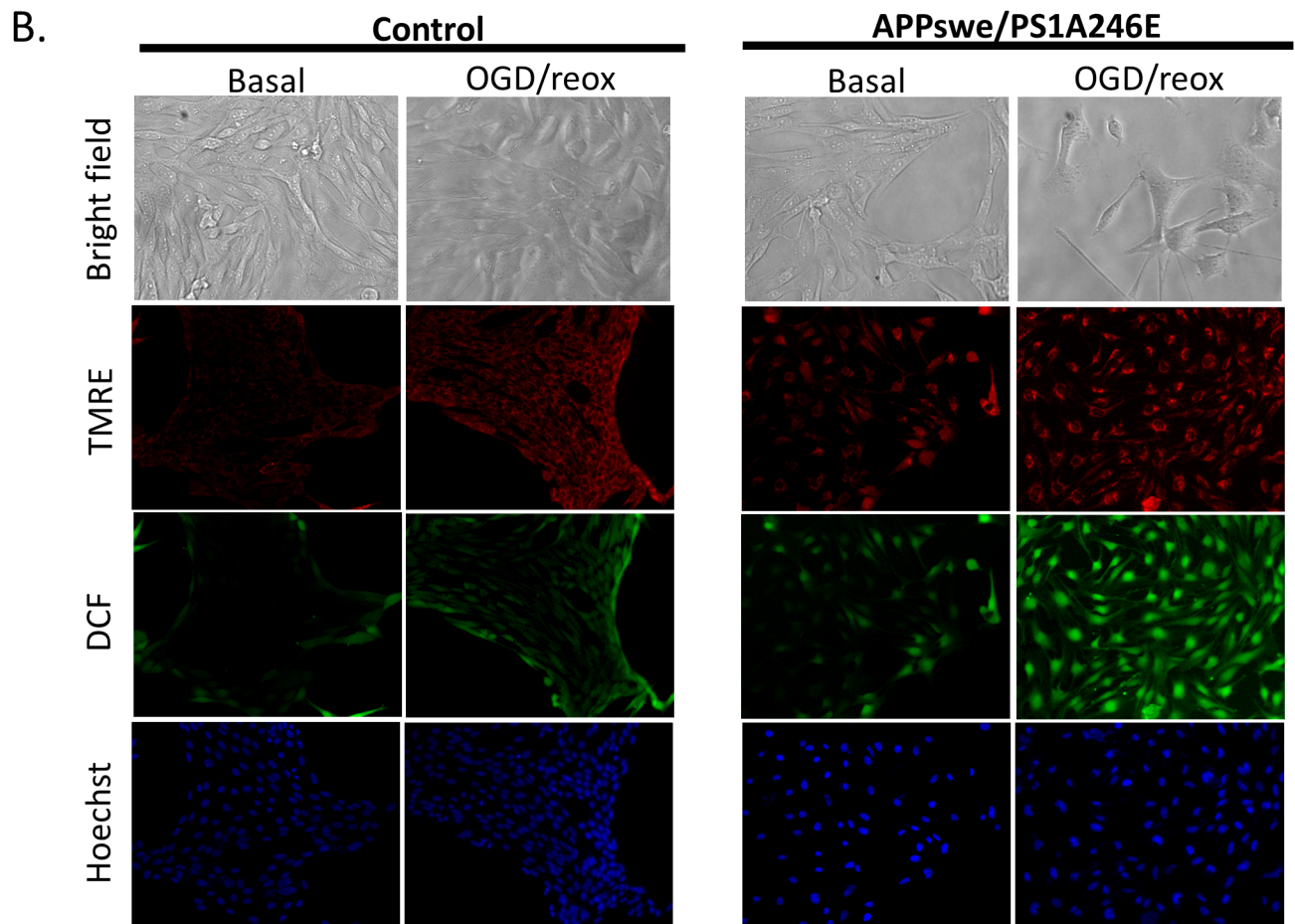
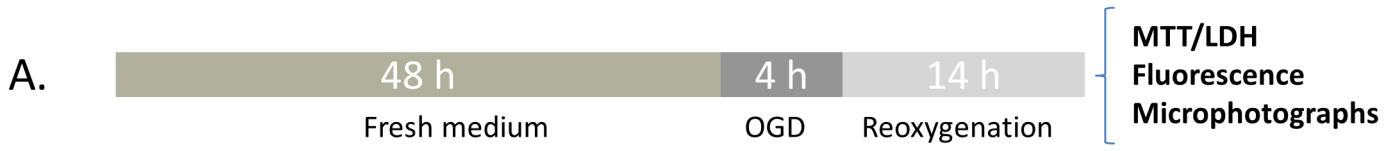
- Abeti, R., Abramov, A. Y. and Duchen, M. R. (2011) Beta-amyloid activates PARP causing astrocytic metabolic failure and neuronal death. *Brain : a journal of neurology*, 134, 1658-1672.**
- Abramov, A. Y., Canevari, L. and Duchen, M. R. (2004) Beta-amyloid peptides induce mitochondrial dysfunction and oxidative stress in astrocytes and death of neurons through activation of NADPH oxidase. *The Journal of neuroscience : the official journal of the Society for Neuroscience*, 24, 565-575.**
- Anderson, M. F., Blomstrand, F., Blomstrand, C., Eriksson, P. S. and Nilsson, M. (2003) Astrocytes and stroke: networking for survival? *Neurochemical research*, 28, 293-305.**
- Beck, S. J., Guo, L., Phensy, A. et al. (2016) Deregulation of mitochondrial F1FO-ATP synthase via OSCP in Alzheimer's disease. *Nature communications*, 7, 11483.**
- Begley, J. G., Duan, W., Chan, S., Duff, K. and Mattson, M. P. (1999) Altered calcium homeostasis and mitochondrial dysfunction in cortical synaptic compartments of presenilin-1 mutant mice. *Journal of neurochemistry*, 72, 1030-1039.**
- Casley, C. S., Canevari, L., Land, J. M., Clark, J. B. and Sharpe, M. A. (2002) Beta-amyloid inhibits integrated mitochondrial respiration and key enzyme activities. *Journal of neurochemistry*, 80, 91-100.**
- Casserly, I. and Topol, E. (2004) Convergence of atherosclerosis and Alzheimer's disease: inflammation, cholesterol, and misfolded proteins. *Lancet*, 363, 1139-1146.**
- Cha, M. Y., Cho, H. J., Kim, C. et al. (2015) Mitochondrial ATP synthase activity is impaired by suppressed O-GlcNAcylation in Alzheimer's disease. *Human molecular genetics*, 24, 6492-6504.**
- Chen, J., Jin, K., Chen, M., Pei, W., Kawaguchi, K., Greenberg, D. A. and Simon, R. P. (1997) Early detection of DNA strand breaks in the brain after transient focal ischemia: implications for the role of DNA damage in apoptosis and neuronal cell death. *Journal of neurochemistry*, 69, 232-245.**
- Chen, Y. and Swanson, R. A. (2003) Astrocytes and brain injury. *Journal of cerebral blood flow and metabolism : official journal of the International Society of Cerebral Blood Flow and Metabolism*, 23, 137-149.**
- Devi, L., Prabhu, B. M., Galati, D. F., Avadhani, N. G. and Anandatheerthavarada, H. K. (2006) Accumulation of amyloid precursor protein in the mitochondrial import channels of human Alzheimer's disease brain is associated with mitochondrial dysfunction. *The Journal of neuroscience : the official journal of the Society for Neuroscience*, 26, 9057-9068.**
- Dragicevic, N., Copes, N., O'Neal-Moffitt, G. et al. (2011) Melatonin treatment restores mitochondrial function in**

- Alzheimer's mice: a mitochondrial protective role of melatonin membrane receptor signaling. *Journal of pineal research*, 51, 75-86.**
- Esteras, N., Rohrer, J. D., Hardy, J., Wray, S. and Abramov, A. Y. (2017) Mitochondrial hyperpolarization in iPSC-derived neurons from patients of FTDP-17 with 10+16 MAPT mutation leads to oxidative stress and neurodegeneration. *Redox biology*, 12, 410-422.**
- Garcia-Dorado, D., Ruiz-Meana, M., Inserte, J., Rodriguez-Sinovas, A. and Piper, H. M. (2012) Calcium-mediated cell death during myocardial reperfusion. *Cardiovascular research*, 94, 168-180.**
- Goldberg, M. P. and Choi, D. W. (1993) Combined oxygen and glucose deprivation in cortical cell culture: calcium-dependent and calcium-independent mechanisms of neuronal injury. *The Journal of neuroscience : the official journal of the Society for Neuroscience*, 13, 3510-3524.**
- Gomez-Gonzalo, M., Martin-Fernandez, M., Martinez-Murillo, R. et al. (2017) Neuron-astrocyte signaling is preserved in the aging brain. *Glia*, 65, 569-580.**
- Gorelick, P. B. (2004) Risk factors for vascular dementia and Alzheimer disease. *Stroke; a journal of cerebral circulation*, 35, 2620-2622.**
- Grolla, A. A., Fakhfouri, G., Balzaretto, G., Marcello, E., Gardoni, F., Canonico, P. L., DiLuca, M., Genazzani, A. A. and Lim, D. (2013) Abeta leads to Ca(2)(+) signaling alterations and transcriptional changes in glial cells. *Neurobiology of aging*, 34, 511-522.**
- Guo, Q., Furukawa, K., Sopher, B. L., Pham, D. G., Xie, J., Robinson, N., Martin, G. M. and Mattson, M. P. (1996) Alzheimer's PS-1 mutation perturbs calcium homeostasis and sensitizes PC12 cells to death induced by amyloid beta-peptide. *Neuroreport*, 8, 379-383.**
- Guo, Q., Sopher, B. L., Furukawa, K., Pham, D. G., Robinson, N., Martin, G. M. and Mattson, M. P. (1997) Alzheimer's presenilin mutation sensitizes neural cells to apoptosis induced by trophic factor withdrawal and amyloid beta-peptide: involvement of calcium and oxyradicals. *The Journal of neuroscience : the official journal of the Society for Neuroscience*, 17, 4212-4222.**
- Hardy, J. and Selkoe, D. J. (2002) The amyloid hypothesis of Alzheimer's disease: progress and problems on the road to therapeutics. *Science*, 297, 353-356.**
- Johnston, J. M., Burnett, P., Thomas, A. P. and Tezapsidis, N. (2006) Calcium oscillations in type-1 astrocytes, the effect of a presenilin 1 (PS1) mutation. *Neuroscience letters*, 395, 159-164.**
- Kalaria, R. N., Bhatti, S. U., Lust, W. D. and Perry, G. (1993) The amyloid precursor protein in ischemic brain injury and chronic hypoperfusion. *Annals of the New York Academy of Sciences*, 695, 190-193.**
- Lee, I., Bender, E. and Kadenbach, B. (2002) Control of mitochondrial membrane potential and ROS formation by**

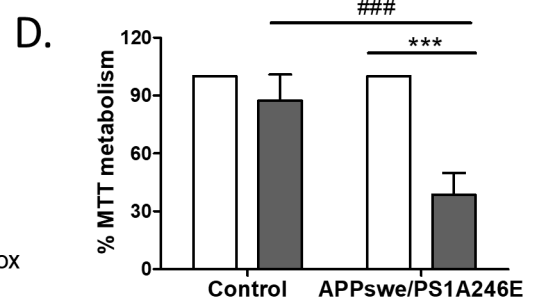
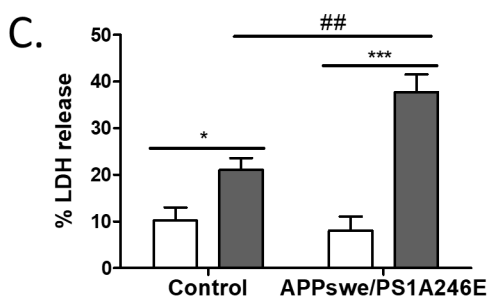
- reversible phosphorylation of cytochrome c oxidase. *Molecular and cellular biochemistry*, 234-235, 63-70.
- Lee, J. M., Zipfel, G. J. and Choi, D. W. (1999) The changing landscape of ischaemic brain injury mechanisms. *Nature*, 399, A7-14.
- Li, Y., Chopp, M., Jiang, N., Yao, F. and Zaloga, C. (1995) Temporal profile of in situ DNA fragmentation after transient middle cerebral artery occlusion in the rat. *Journal of cerebral blood flow and metabolism : official journal of the International Society of Cerebral Blood Flow and Metabolism*, 15, 389-397.
- Li, Y., Liu, Z., Xin, H. and Chopp, M. (2014) The role of astrocytes in mediating exogenous cell-based restorative therapy for stroke. *Glia*, 62, 1-16.
- Liu, Y., Peterson, D. A., Kimura, H. and Schubert, D. (1997) Mechanism of cellular 3-(4,5-dimethylthiazol-2-yl)-2,5-diphenyltetrazolium bromide (MTT) reduction. *Journal of neurochemistry*, 69, 581-593.
- Murphy, E., Pan, X., Nguyen, T., Liu, J., Holmstrom, K. M. and Finkel, T. (2014) Unresolved questions from the analysis of mice lacking MCU expression. *Biochemical and biophysical research communications*, 449, 384-385.
- Nagele, R. G., D'Andrea, M. R., Lee, H., Venkataraman, V. and Wang, H. Y. (2003) Astrocytes accumulate A beta 42 and give rise to astrocytic amyloid plaques in Alzheimer disease brains. *Brain research*, 971, 197-209.
- Olabarria, M., Noristani, H. N., Verkhatsky, A. and Rodriguez, J. J. (2010) Concomitant astroglial atrophy and astrogliosis in a triple transgenic animal model of Alzheimer's disease. *Glia*, 58, 831-838.
- Ortega-Martinez, S. (2015) Dexamethasone acts as a radiosensitizer in three astrocytoma cell lines via oxidative stress. *Redox biology*, 5, 388-397.
- Panickar, K. S. and Norenberg, M. D. (2005) Astrocytes in cerebral ischemic injury: morphological and general considerations. *Glia*, 50, 287-298.
- Paris, D., Patel, N., DelleDonne, A., Quadros, A., Smeed, R. and Mullan, M. (2004a) Impaired angiogenesis in a transgenic mouse model of cerebral amyloidosis. *Neuroscience letters*, 366, 80-85.
- Paris, D., Townsend, K., Quadros, A. et al. (2004b) Inhibition of angiogenesis by Abeta peptides. *Angiogenesis*, 7, 75-85.
- Pasquier, F., Leys, D. and Scheltens, P. (1998) The influence of coincidental vascular pathology on symptomatology and course of Alzheimer's disease. *Journal of neural transmission. Supplementum*, 54, 117-127.
- Pluta, R. (2004a) Alzheimer lesions after ischemia-reperfusion brain injury. *Folia neuropathologica / Association of Polish Neuropathologists and Medical Research Centre, Polish Academy of Sciences*, 42, 181-186.
- Pluta, R. (2004b) From brain ischemia-reperfusion injury to possible sporadic Alzheimer's disease. *Current neurovascular research*, 1, 441-453.

- Rodriguez, J. J., Olabarria, M., Chvatal, A. and Verkhratsky, A. (2009) Astroglia in dementia and Alzheimer's disease. *Cell death and differentiation*, 16, 378-385.
- Rossi, D. J., Oshima, T. and Attwell, D. (2000) Glutamate release in severe brain ischaemia is mainly by reversed uptake. *Nature*, 403, 316-321.
- Rothstein, J. D., Dykes-Hoberg, M., Pardo, C. A. et al. (1996) Knockout of glutamate transporters reveals a major role for astroglial transport in excitotoxicity and clearance of glutamate. *Neuron*, 16, 675-686.
- Schmidt, C., Lepsverdize, E., Chi, S. L., Das, A. M., Pizzo, S. V., Dityatev, A. and Schachner, M. (2008) Amyloid precursor protein and amyloid beta-peptide bind to ATP synthase and regulate its activity at the surface of neural cells. *Molecular psychiatry*, 13, 953-969.
- Schneider, I., Reverse, D., Dewachter, I. et al. (2001) Mutant presenilins disturb neuronal calcium homeostasis in the brain of transgenic mice, decreasing the threshold for excitotoxicity and facilitating long-term potentiation. *The Journal of biological chemistry*, 276, 11539-11544.
- Serrano, J., Fernandez, A. P., Martinez-Murillo, R. and Martinez, A. (2010) High sensitivity to carcinogens in the brain of a mouse model of Alzheimer's disease. *Oncogene*, 29, 2165-2171.
- Seyfried, T. N., el-Abbadi, M. and Roy, M. L. (1992) Ganglioside distribution in murine neural tumors. *Molecular and chemical neuropathology*, 17, 147-167.
- Sheppard, C. A., Simpson, P. B., Sharp, A. H., Nucifora, F. C., Ross, C. A., Lange, G. D. and Russell, J. T. (1997) Comparison of type 2 inositol 1,4,5-trisphosphate receptor distribution and subcellular Ca²⁺ release sites that support Ca²⁺ waves in cultured astrocytes. *Journal of neurochemistry*, 68, 2317-2327.
- Sompol, P., Ittarat, W., Tangpong, J., Chen, Y., Doubinskaia, I., Batinic-Haberle, I., Abdul, H. M., Butterfield, D. A. and St Clair, D. K. (2008) A neuronal model of Alzheimer's disease: an insight into the mechanisms of oxidative stress-mediated mitochondrial injury. *Neuroscience*, 153, 120-130.
- Swanson, R. A., Ying, W. and Kauppinen, T. M. (2004) Astrocyte influences on ischemic neuronal death. *Current molecular medicine*, 4, 193-205.
- Verkhratsky, A., Olabarria, M., Noristani, H. N., Yeh, C. Y. and Rodriguez, J. J. (2010) Astrocytes in Alzheimer's disease. *Neurotherapeutics : the journal of the American Society for Experimental NeuroTherapeutics*, 7, 399-412.
- Weiss, J. H., Pike, C. J. and Cotman, C. W. (1994) Ca²⁺ channel blockers attenuate beta-amyloid peptide toxicity to cortical neurons in culture. *Journal of neurochemistry*, 62, 372-375.
- Zhao, Y. and Rempe, D. A. (2010) Targeting astrocytes for stroke therapy. *Neurotherapeutics : the journal of the American Society for Experimental NeuroTherapeutics*, 7, 439-451.

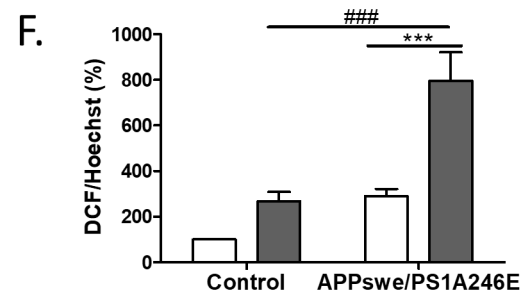
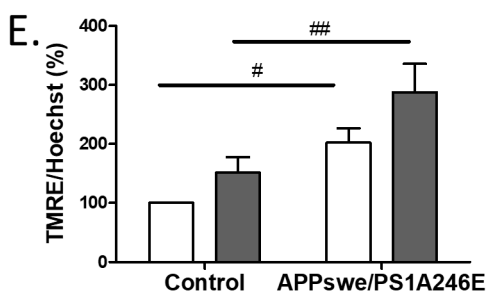
Zhen, G., Kim, Y. T., Li, R. C. et al. (2012) PGE2 EP1 receptor exacerbated neurotoxicity in a mouse model of cerebral ischemia and Alzheimer's disease. *Neurobiology of aging*, 33, 2215-2219.

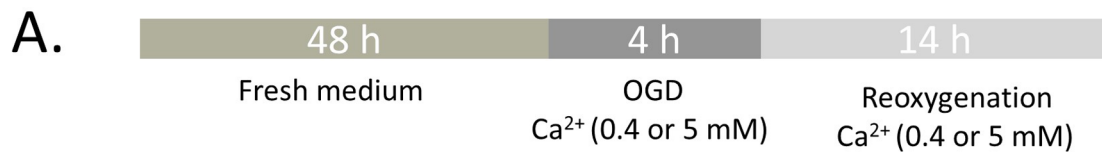


Cell viability

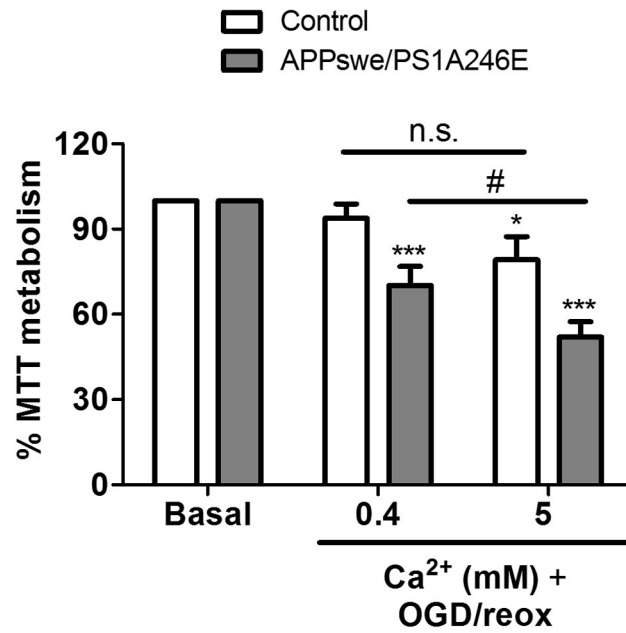


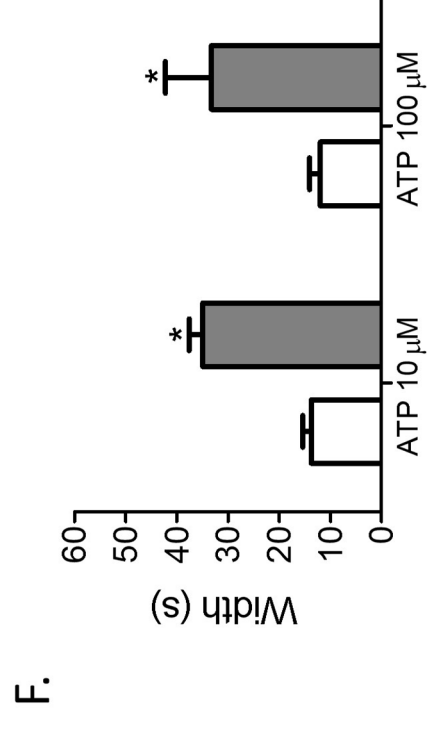
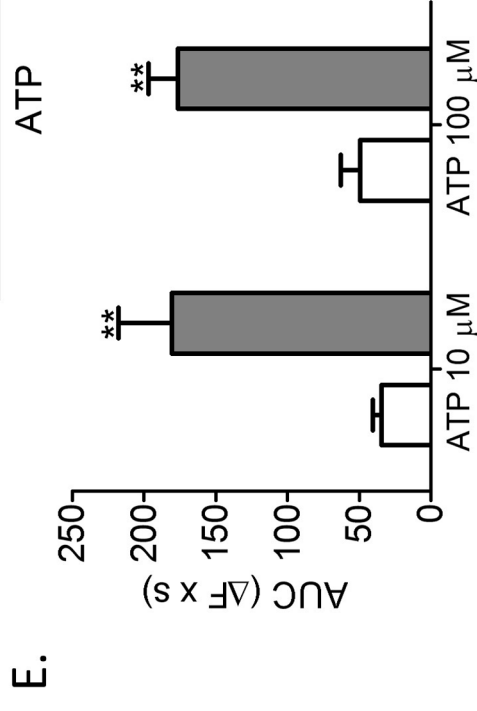
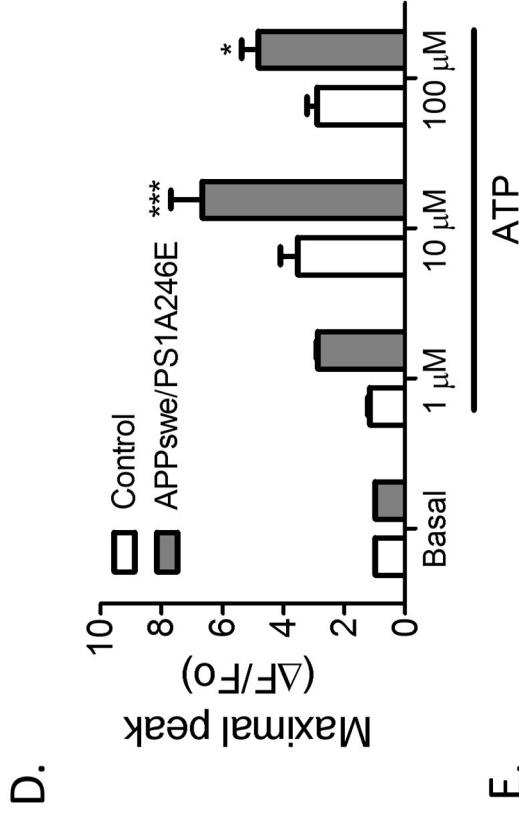
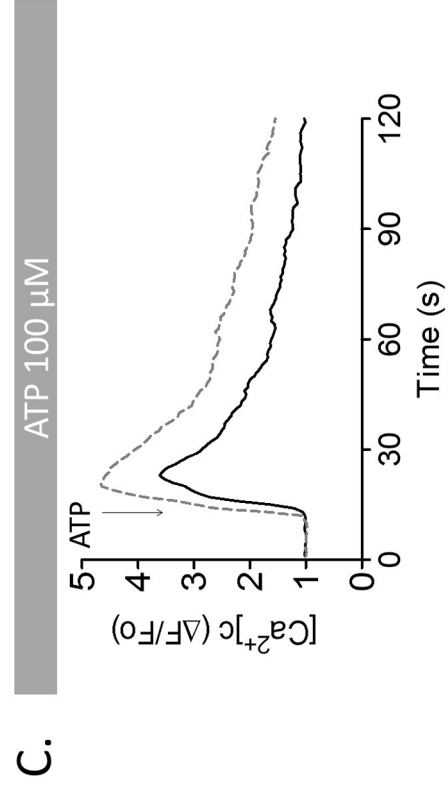
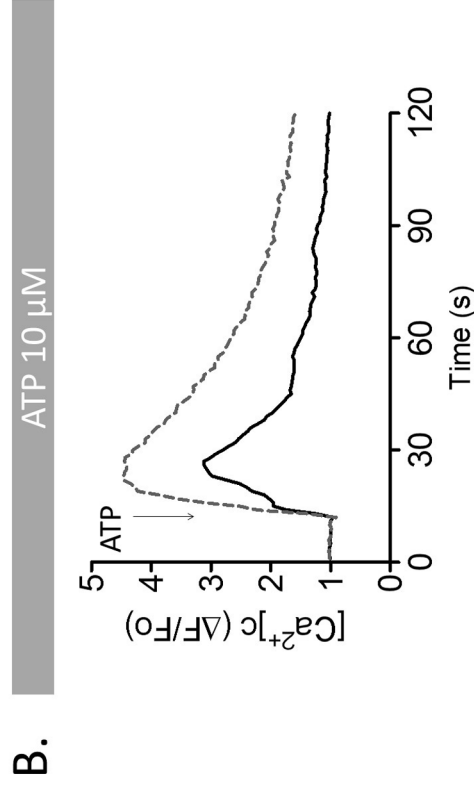
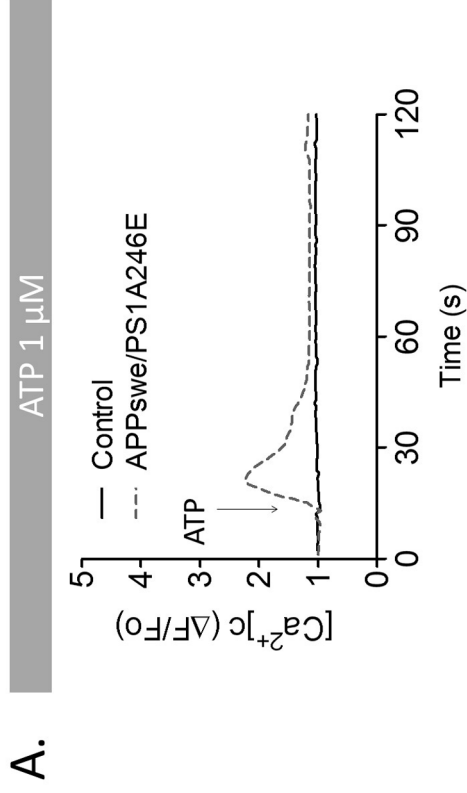
Fluorescence measurements

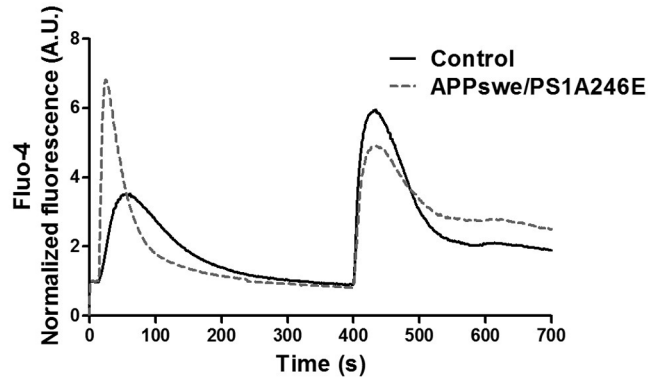
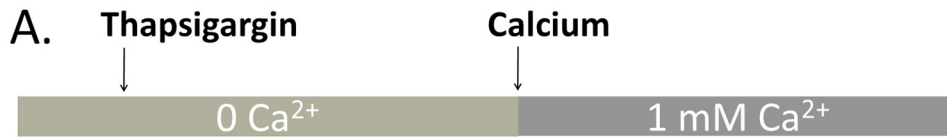




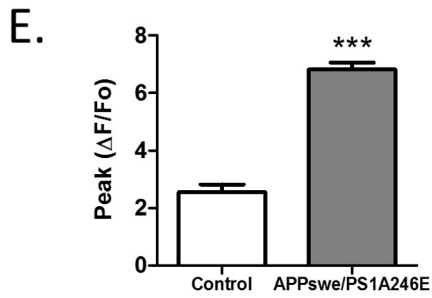
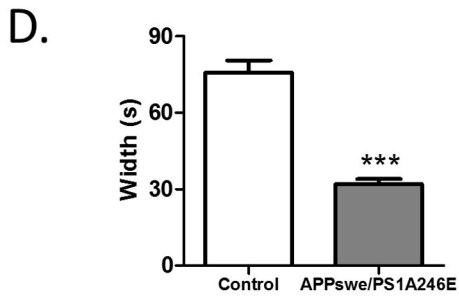
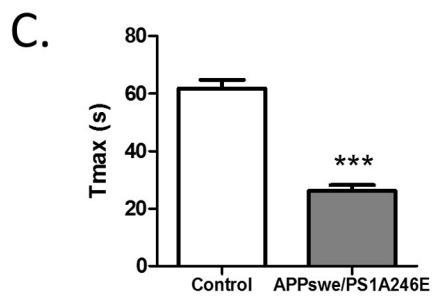
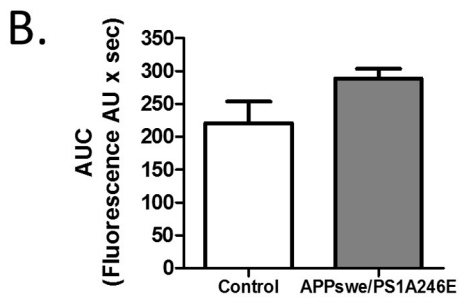
B. Cell viability



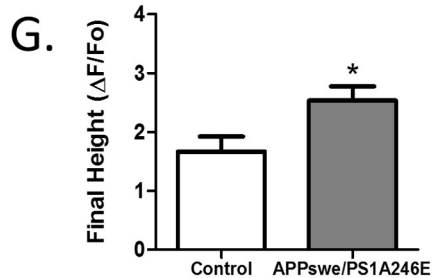
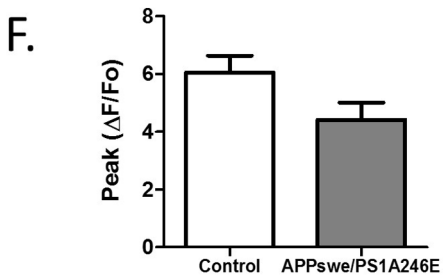




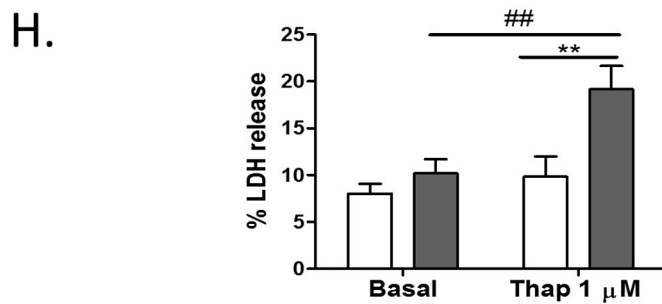
Thapsigargin



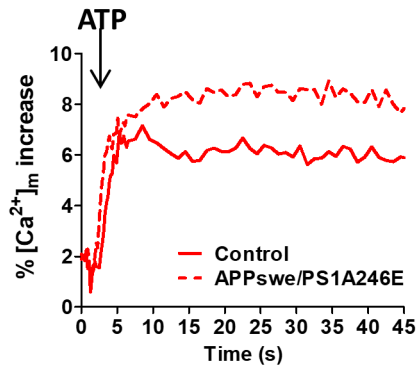
CCE



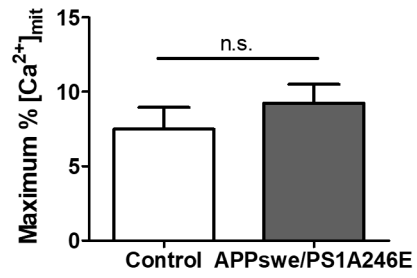
Viability



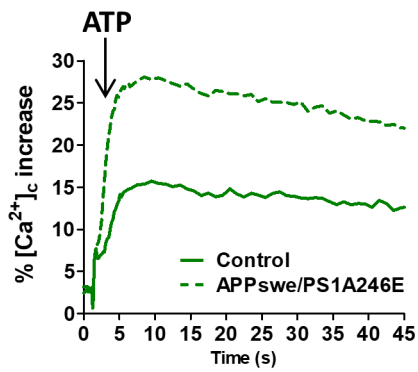
A.



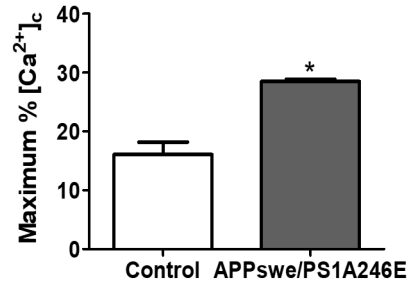
B.



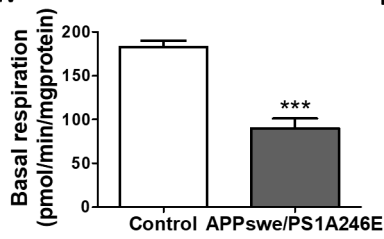
C.



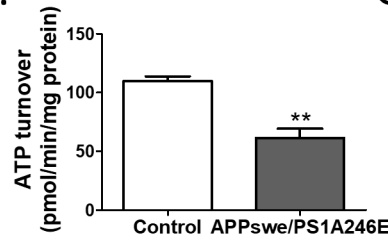
D.



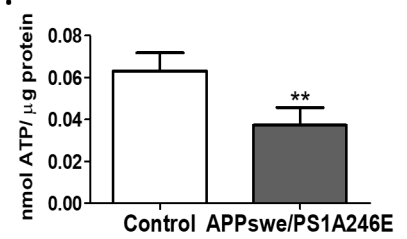
E.



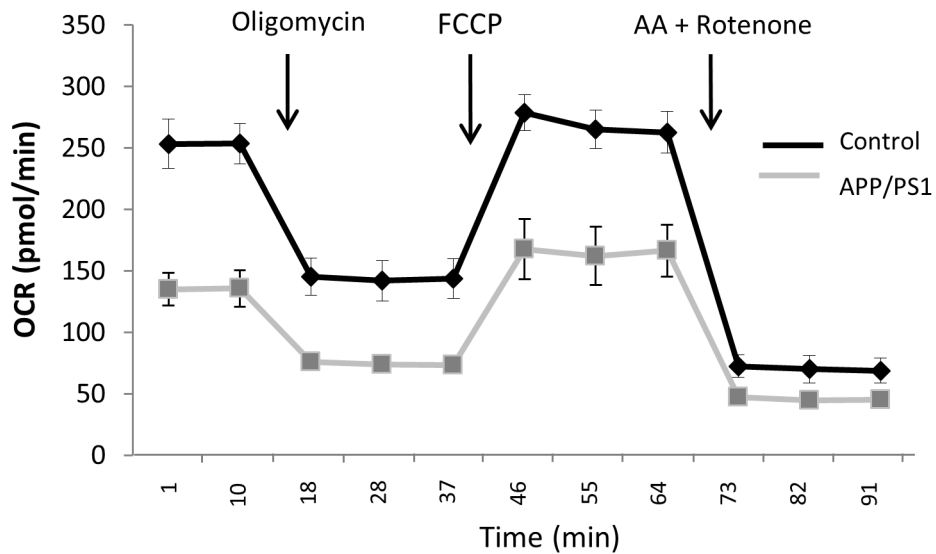
F.

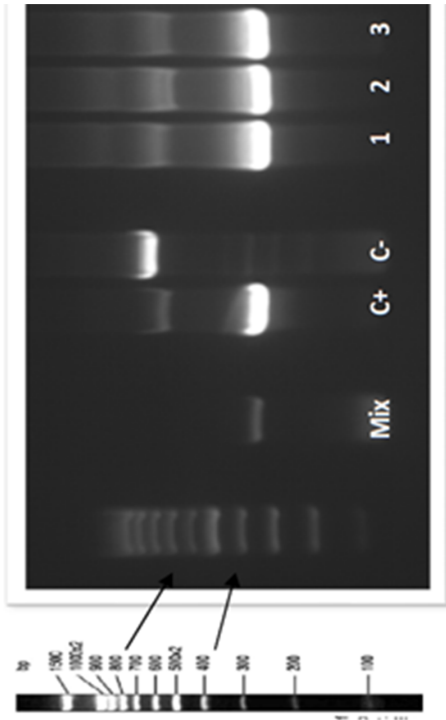


G.

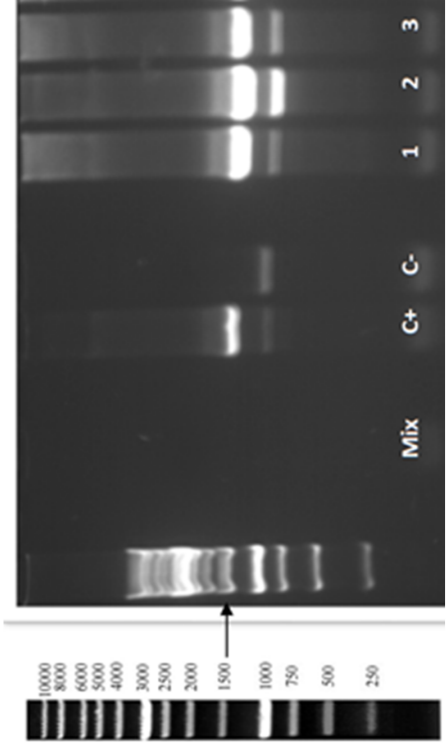


H.



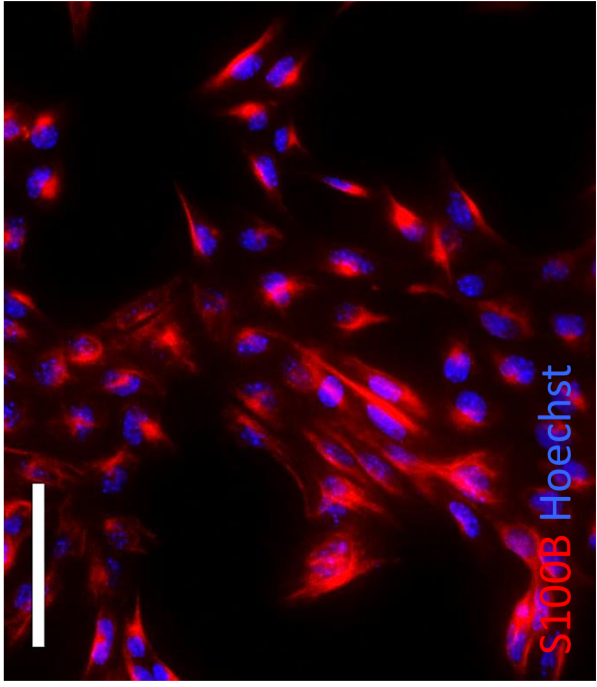


APP mutation

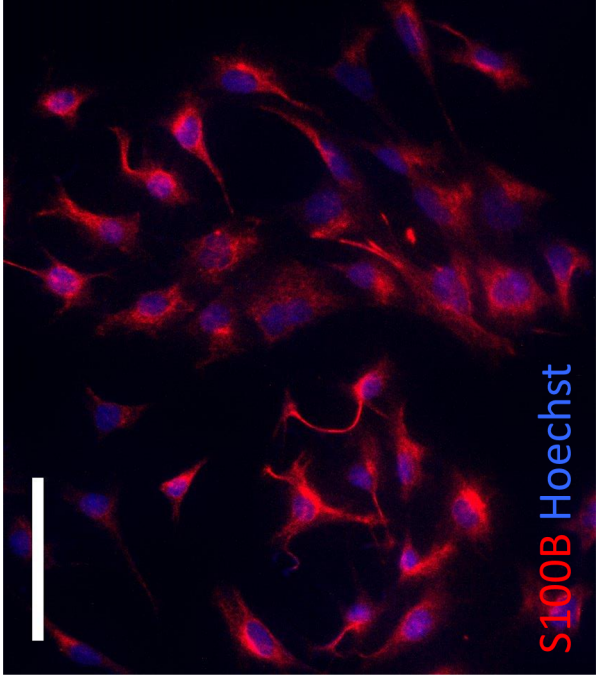


PS1 mutation

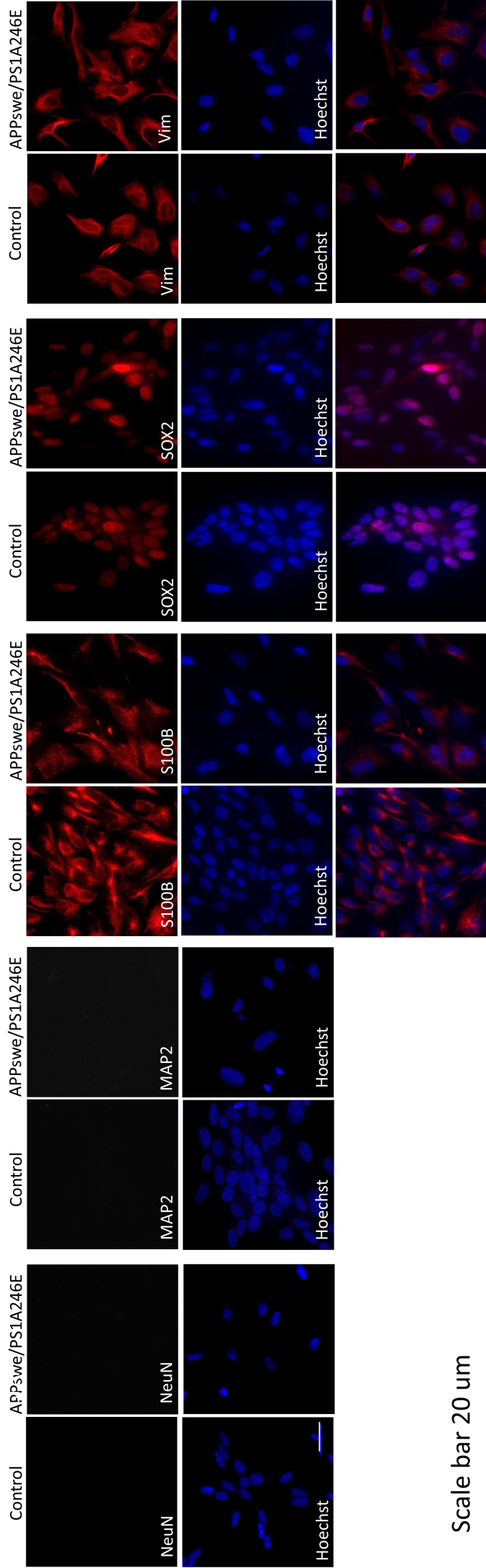
Control



APP/PS1



Scale bar 50 μ m



Scale bar 20 um